

## Single-Electron Charging in Double and Triple Quantum Dots with Tunable Coupling

F. R. Waugh, M. J. Berry, D. J. Mar, and R. M. Westervelt

*Division of Applied Sciences and Department of Physics, Harvard University, Cambridge, Massachusetts 02138*

K. L. Campman and A. C. Gossard

*Materials Department, University of California, Santa Barbara, California 93106*

(Received 26 August 1994)

We report low-temperature tunneling measurements at zero magnetic field through double and triple quantum dots with adjustable interdot coupling, fabricated in a GaAs/AlGaAs heterostructure. As the coupling is increased, Coulomb blockade conductance peaks split into two (double dot) or three (triple dot) peaks each. The splitting tracks closely the measured tunnel conductance and experimentally determines the total interaction energy. Coupled double and triple dots with different gate capacitance show quasiperiodic beating.

PACS numbers: 73.20.Dx, 71.45.-d, 73.40.Gk

Submicron quantum dots have potential as “artificial atoms” and artificial molecules and for “single electronics” in which individual electrons represent bits of information [1–5]. Crucial to both fields is an understanding of how coupled dots interact. Experiments on the conductance of “artificial crystals” defined in a two-dimensional electron gas by two modulated gates show evidence for energy band formation in strong magnetic fields and sharp conductance peaks near threshold [6,7]. Many interesting phenomena have been predicted for coupled quantum dot arrays in the tunneling regime [4,8–12], including conductance peak splitting, peak suppression, single-electron solitons, and quasiperiodicity. A single dot interacting with its leads [13,14] and recently coupled double dots [15,16] have been studied experimentally.

In this Letter, we report low-temperature tunneling measurements at zero magnetic field through double and triple quantum dot arrays defined in a two-dimensional electron gas by tunable gates, which permit separate control of the tunnel barriers and wall positions to compensate for disorder. Figure 1(a) shows a scanning electron beam (SEM) micrograph of a 14-gate triple-dot device of this type, described in detail below. As the quantum point contacts joining dots are opened, the interdot tunnel conductance increases in a continuous transition from isolated dots to one large dot. Isolated dot arrays show strong Coulomb blockade conductance peaks vs. gate voltage which split into two (double dot) and three (triple dot) peaks as the coupling increases. The splitting is proportional to the measured barrier conductance and experimentally determines the total interaction energy due to classical interdot capacitance and quantum tunneling. For dot arrays with unequal gate capacitance, the conductance peaks exhibit beating and quasiperiodicity predicted by theory [8].

To understand these experiments, consider two or three identical dots weakly coupled to external leads, so that the total number of electrons  $N_{\text{tot}} = \sum N_i$  is a good quantum number. If the interdot tunneling rate is also weak, then the  $N_i$  for each dot are also good quantum

numbers and the “orthodox” theory of single electron charging [3,4] applies: The energy of a single dot is the charging energy  $U = (Ne - C_g V_g)^2 / 2C_\Sigma$  plus the sum over single-particle states  $E_n$ , where  $C_g$  and  $V_g$  are the gate capacitance and voltage, and  $C_\Sigma$  is the total capacitance. We first consider the case where the

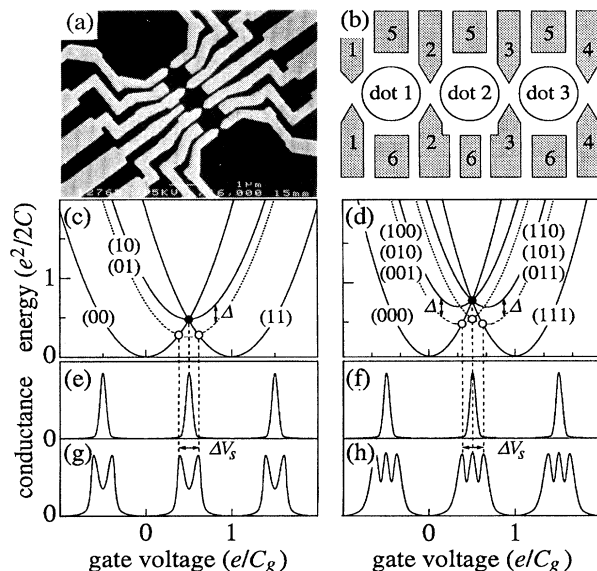


FIG. 1. (a) SEM micrograph at 16000 $\times$  magnification of three coupled quantum dots with tunable tunneling barriers in GaAs/AlGaAs heterostructure. Scale bar is 1  $\mu\text{m}$ ; dots are  $0.5 \times 0.8 \mu\text{m}^2$ . (b) Dot and gate labeling. (c) Double-dot and (d) triple-dot charging energy vs gate voltage for indicated numbers ( $N_1 N_2 \dots$ ) of electrons on each dot for identical dots. Without interdot coupling, parabolas with unequal  $N_i$  are degenerate (solid curves). Coupling removes degeneracy, shifting lowest parabola down by  $\Delta$  (dotted curves). (e) Double-dot and (f) triple-dot conductance vs gate voltage without coupling (schematic). Conductance peaks occur at filled markers in (c) and (d). (g) Double-dot and (h) triple-dot conductance vs gate voltage with coupling (schematic). Conductance peaks occur at open markers in (c) and (d). Coupling splits peaks, with split peak separation  $\Delta V_s \propto \Delta$  for small  $\Delta$ .

interdot tunneling rate and the interdot capacitances  $C_{ij}$  are negligible. Corresponding to the experiment below, we take  $E_F > U > \Delta E > k_B T$ , with  $E_F$  being the Fermi energy and  $\Delta E$  being the average level spacing. At these low temperatures, the ground state for each dot charge configuration ( $N_1 N_2 \dots$ ), shown as the solid curves in Figs. 1(c) and 1(d), dominates equilibrium transport. When  $N_{\text{tot}}$  is not an integer multiple of the number of dots, the dot system is internally polarized, and the corresponding set of degenerate parabolas have higher energy as indicated in Figs. 1(c) and 1(d). A single conductance peak occurs where the parabolas for different  $N_{\text{tot}}$  intersect, corresponding to sequential tunneling from dot to dot.

As illustrated in Fig. 1, conductance peaks split if interdot tunneling or interdot capacitance is no longer negligible. Interdot tunneling mixes single dot quantum states, producing new states of the entire coupled dot array. Because of internal polarization, the total Coulomb energy can no longer be represented by a simple capacitive term as in the orthodox theory. For a simple two-site model, one array state moves down in energy with tunneling rate and one moves up. The actual situation is more complex, because tunneling can occur between a range of single-particle states on each dot, so that the previously degenerate dot states are expected to open into a manifold of array states, covering a range of energies determined by the tunneling rate. The array ground state for a given  $N_{\text{tot}}$ , which dominates transport at low temperatures, normally moves downward as tunneling destroys the internal polarization, as indicated schematically by the dashed curves in Figs. 1(c) and 1(d), producing conductance peak splitting  $\Delta V_s = (2C_\Sigma/C_g e)\Delta$  indicated in Figs. 1(g) and 1(h). The peak splitting must physically saturate when the dots merge into one for strong tunneling. The interaction energy  $\Delta$  has been found for Hubbard model calculations [11,12] for small numbers of single-particle levels and weak tunneling.

Classical interdot capacitance also reduces the energy of polarized charge configurations [8] of identical dots and produces peak splitting. A purely capacitive description of dot interactions, however, requires that the classical interdot capacitance increase strongly with coupling while the interdot tunneling remains negligible; we argue below that this is not the case for our experiments. For mismatched dots, single electron charging theory [8] predicts peak suppression due to the "stochastic" Coulomb blockade. We observe this phenomenon for mismatched dots, as shown below, and find that the suppression is lifted by strong interdot tunneling.

We studied two devices: a triple dot (device A) shown in Fig. 1(a), used also for double-dot experiments by not energizing all gates, and a similar double dot (device B). All results below are for device A unless otherwise noted. Both devices were fabricated using the same GaAs/AlGaAs heterostructure, which contains a two-dimensional electron gas located 470 Å beneath the

surface with sheet density  $3.7 \times 10^{11} \text{ cm}^{-2}$  and mobility  $5 \times 10^5 \text{ cm}^2/\text{Vs}$  at 10 K, and phase coherence length  $>20 \mu\text{m}$  for  $T < 1 \text{ K}$  [17]. Device A consists of 14 Schottky gates fabricated with electron-beam lithography and chrome/gold evaporation on the heterostructure surface. As shown in Figs. 1(a) and 1(b), eight gates form the four quantum point contacts used as tunnel barriers and six gates form the dot confining walls when sufficient negative voltage is applied to deplete the electron gas underneath. The lithographic size of each dot is  $0.5 \times 0.8 \mu\text{m}^2$ . As depicted in Fig. 1(b), the device is wired with six independently tunable gate voltages: one for each tunnel barrier ( $V_1$  through  $V_4$ ) and one each for each set of confining walls at the top ( $V_5$ ) and bottom ( $V_6$ ) of the array; note that the confining wall on dot 2 and gate 6 is intentionally made smaller than the others. Double-dot experiments were conducted using device A by not energizing  $V_1$ . The samples were cooled in a He dilution refrigerator at the base temperature  $T = 14 \text{ mK}$ ; care was taken to shield the samples from external electromagnetic radiation. The tunneling conductance of dot arrays was measured by applying a small (typically 5 to 10  $\mu\text{V}$ ) ac voltage and recording the current with a current preamplifier and lock-in amplifier.

An important advantage of quantum dots shown in Fig. 1(a) is that each element of the device is controlled by separate gates and can be individually tested and adjusted. This tunability permits compensation for disorder, particularly important for the tunnel barriers, and distinguishes our devices from previously studied semiconductor dot arrays [6,7] and coupled metal islands [18,19]. For device A, each of the four nominally identical point contacts, separately measured, show high quality characteristics with up to 10 quantized conductance plateaus. However, their pinchoff voltages range from  $-0.92$  to  $-1.02 \text{ V}$ , demonstrating the need for independent tunability. When separately energized, each dot shows regularly spaced conductance peaks corresponding to adding a single electron as gate voltages 5 and 6 are swept [1,2]. The peak spacings  $\Delta V_{ia}$  for dot  $i$  when gate  $a$  is swept determine the gate capacitances  $C_{ia} = e/\Delta V_{ia}$  of  $C_{15} = 38 \text{ aF}$ ,  $C_{25} = 43 \text{ aF}$ ,  $C_{35} = 41 \text{ aF}$ ,  $C_{16} = 41 \text{ aF}$ ,  $C_{26} = 32 \text{ aF}$ , and  $C_{36} = 39 \text{ aF}$ . Analysis of current-voltage characteristics and of conductance peak linewidths at temperatures between base and 400 mK for a single dot of the array yields  $C_\Sigma \cong 0.4 \text{ fF}$ ,  $e^2/2C_\Sigma \cong 200 \mu\text{eV}$ ,  $\Delta E \sim 30 \mu\text{eV}$ , and  $k_B T_e \cong 5$  to  $10 \mu\text{eV}$ , where  $T_e$  is the electron temperature. The conductance peak height increases at lower temperature to  $T < 50 \text{ mK}$ . These observations indicate that the dots are in the fully quantum regime with  $E_F > U > \Delta E > k_B T$  [1,2].

Figures 2(a)–2(d) show changes in the conductance  $G_{dd}$  of a double dot vs gate voltage  $V_5$  with increasing interdot coupling controlled by  $V_3$ ; the double dot is formed by grounding gate 1 and energizing all other gates. In Fig. 2(a), the interdot coupling is weak, and the double-dot conductance consists of weakly split peaks with the

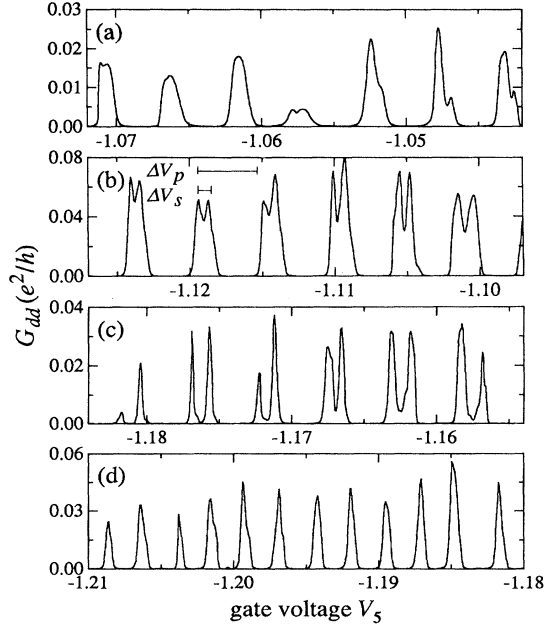


FIG. 2. Double-dot conductance  $G_{dd}$  vs gate voltage  $V_5$  for increasing interdot coupling. Coupling splits conductance peaks, with split peak separation  $\Delta V_s$  proportional to interaction energy  $\Delta$ . Interdot barrier conductance in units  $e^2/h$  is (a) 0.03, (b) 0.88, (c) 1.37, and (d) 1.94, estimated by shifting measured point contact conductance by 72 mV to account for influence of nearby gates.

same separation  $\Delta V_p$  measured individually for single dots 2 and 3. In Figs. 2(b) and 2(c), each peak clearly splits into two peaks, whose separation increases with interdot coupling. Finally, in Fig. 2(d), the conductance is that of a single large dot with peak separation about half that in Fig. 2(a), when the tunnel barrier between dots 2 and 3 is removed. Similar behavior is observed in device B. While uncontrolled peak splitting attributed to disorder has been observed [20–22], regular peak splitting controlled via tunable gates has not previously been reported [15,16].

Figures 3(a) and 3(b) demonstrate the strong correlation between peak splitting and interdot tunnel conductance. Figure 3(a) plots the fractional peak splitting  $F = 2\Delta V_s/\Delta V_p$  [see Fig. 2(b)] averaged over 16 sweeps of gate voltage  $V_5$  vs gate voltage  $V_3$ . The tunnel barrier conductance  $G_b$ , separately measured, is also plotted in Fig. 3(a), offset by 72 mV to account for the influence of other gates. As shown, the fractional peak splitting and tunnel conductance track each other closely. Coherent coupling of electron states on separate dots can occur, because  $k_B T < \Delta E$ , and the phase coherence length is much larger than the dot size [17]. This correlation is shown in another way in Fig. 3(b), which plots the double-dot conductance  $G_{dd}$  vs barrier voltage  $V_3$  for fixed gate voltages  $V_5$  and  $V_6$ , together with measured tunnel conductance  $G_b$ ; the fractional peak splittings are shown as triangles. As shown in Fig. 3(a), the peak splitting saturates when the

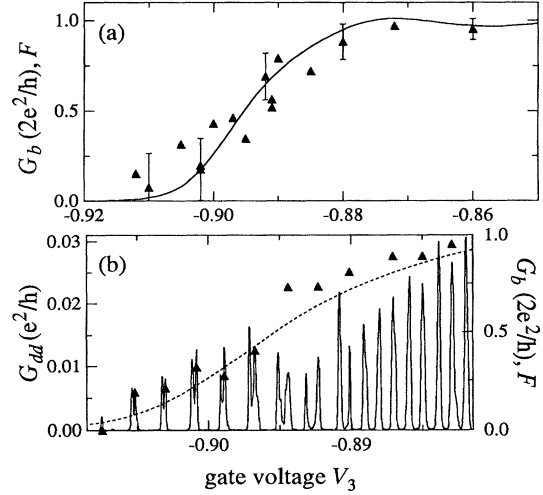


FIG. 3. Double-dot fractional splitting  $F = 2\Delta V_s/\Delta V_p$  (triangles), averaged over 16 sweeps of  $V_5$ , and measured interdot barrier conductance  $G_b$  (curve) vs gate voltage  $V_3$ .  $\Delta V_s$  and  $\Delta V_p$  are defined in Fig. 2(b). (b) Double-dot conductance  $G_{dd}$  (solid curve, left scale),  $F$  (triangles, right scale), and  $G_b$  (dotted curve, right scale) vs gate voltage  $V_3$ .

interdot conductance reaches  $2e^2/h$ ; for this value the two dots merge, and the number of electrons on dot 2 or 3 (separately) is no longer well defined. The corresponding range of energy shifts is  $\Delta \sim 0$  to  $e^2/2C_\Sigma \cong 200 \mu\text{eV}$ , using  $C_\Sigma \cong 0.4$  fF (single dot) and assuming that the raised parabola shifts rigidly downward as in Fig. 1(c).

Numerical simulations [23] of a classical charging model [8] can also give peak splittings similar to experiment. To fit the data, however, requires interdot capacitances which increase strongly with coupling, unlike the classical capacitance for our geometry [24], to values greater than the *total* capacitance  $C_\Sigma$  measured for single dots. Furthermore, the tunneling rate is assumed to be negligible, while the actual measured tunnel conductance is  $\sim e^2/h$ . For similar reasons, the reported strong increase in effective dot-to-lead capacitance of single dots, as the quantum point contacts are opened [13], is most likely a quantum effect controlled by tunneling [14].

Figure 4 illustrates the changes in the conductance  $G_{dd}$  of a double dot using intentionally mismatched gate capacitances  $C_{26}$  and  $C_{36}$ , both controlled by  $V_6$ . Figures 4(a) and 4(b) plot  $G_{dd}$  vs gate voltage  $V_6$  for two values of increasing interdot coupling controlled by  $V_3$ . As before, the conductance peaks show splitting which increases with interdot coupling. Figure 4(a) demonstrates the stochastic Coulomb blockade [8] in which conductance peaks through double dots with different gate capacitance become increasingly sparse at low temperatures. The stochastic Coulomb blockade is suppressed with increased interdot coupling, as shown in Fig. 4(b); this suppression must occur when strong tunneling joins separate dots into one. The measured quasiperiodic beat period of 23 mV for Fig. 4(b) equals the period  $e/(C_{36} - C_{26}) = 23$  mV calculated with the gate capacitances measured for

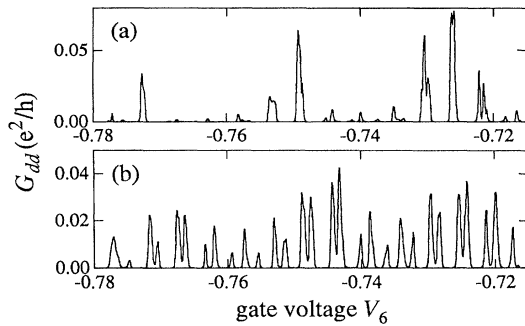


FIG. 4. Double-dot conductance  $G_{dd}$  vs gate voltage  $V_6$  for interdot barrier conductance in units  $e^2/h$  of (a) 0.29 and (b) 1.42. Gate capacitance mismatch causes peak suppression in (a) and quasiperiodic beating in (b).

the singly energized dots. When the gate capacitances are more nearly matched, the beat period is longer and these phenomena become less prominent. For the top gates, designed with similar capacitances, beating is sometimes observed with a period 70 mV, in good agreement with the expected period  $e/(C_{25} - C_{35}) = 80$  mV. No beating is observed in device B, for which the measured gate capacitances are equal to within a few percent.

We have also investigated the triple dot formed by energizing all gates of device A. The triple-dot conductance  $G_{td}$  is plotted vs gate voltage in Fig. 5 for the cases where the gate capacitances are similar [gate voltage  $V_5$  in Fig. 5(a)] and different [gate voltage  $V_6$  in Fig. 5(b)], both with comparable interdot coupling. In Fig. 5(a), each peak splits into three; the slight mismatch of gate capacitances  $C_{15}$ ,  $C_{25}$ , and  $C_{35}$  is observable as an asymmetry of the split peaks. In Fig. 5(b), quasiperiodic beating appears due to the intentional mismatch of gate capacitance  $C_{26}$ . The observed beat periods, 87 mV for the data of Fig. 5(a) and 26 mV in Fig. 5(b), agree well with the capacitances measured from single-dot data and the double-dot beat periods given above.

We thank B.I. Halperin, J. Golden, G. Klimeck, Y. Meir, and S. Trugman for helpful discussions, and A. Adourian, J. Baskey, J. Hergenrother, J. Katine,

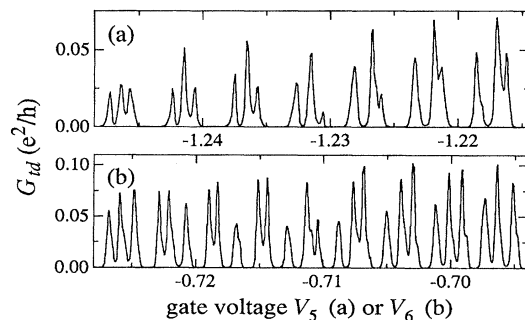


FIG. 5. Triple-dot conductance  $G_{td}$  vs gate voltages (a)  $V_5$  and (b)  $V_6$ . Coupling splits conductance peaks into three in (a); gate capacitance mismatch causes quasiperiodic beating in (b).

D. Ralph, and S. Yang for experimental assistance. This research was supported at Harvard by the ONR under Grant N00014-89-J-1592, by the NSF under Grant DMR-91-19386, and by ARPA under Grant AFOSR-F49620-92-J-0466, and at UCSB by AFOSR-91-0214.

*Note added.*—After submitting this paper, we received two preprints [25,26] calculating how fractional peak splitting depends on barrier conductance for tunnel-coupled double dots. The calculations agree well with the data of Fig. 3.

- [1] M. A. Kastner, *Rev. Mod. Phys.* **64**, 849 (1992), and references therein.
- [2] H. van Houten, C. W. J. Beenakker, and A. A. M. Staring, in *Single Charge Tunneling*, edited by H. Grabert and M. H. Devoret (Plenum, New York, 1992), and references therein.
- [3] I. O. Kulik and R. I. Shekhter, *Sov. Phys. JETP* **41**, 308 (1975).
- [4] D. V. Averin and K. K. Likharev, in *Mesoscopic Phenomena in Solids*, edited by B. L. Altshuler, P. A. Lee, and R. A. Webb (North-Holland, Elsevier, Amsterdam, 1991).
- [5] D. V. Averin and K. K. Likharev, in *Single Charge Tunneling* (Ref. [2]).
- [6] L. P. Kouwenhoven *et al.*, *Phys. Rev. Lett.* **65**, 361 (1990).
- [7] R. J. Haug, J. M. Hong, and K. Y. Lee, *Surf. Sci.* **263**, 415 (1992).
- [8] I. M. Ruzin *et al.*, *Phys. Rev. B* **45**, 13 469 (1992).
- [9] C. Y. Fong *et al.*, *Phys. Rev. B* **46**, 9538 (1992).
- [10] G. W. Bryant, *Phys. Rev. B* **48**, 8024 (1993).
- [11] C. A. Stafford and S. Das Sarma, *Phys. Rev. Lett.* **72**, 3590 (1994).
- [12] G. Klimeck, G. Chen, and S. Datta, *Phys. Rev. B* **50**, 2316 (1994).
- [13] E. B. Foxman *et al.*, *Phys. Rev. B* **47**, 10 020 (1993).
- [14] G. Falci *et al.*, *Physica (Amsterdam)* **203B**, 409 (1994); *Phys. Rev. Lett.* **74**, 3257 (1995); K. A. Matveev, *Phys. Rev. B* **51**, 1743 (1995).
- [15] M. Kemerink and L. W. Molenkamp, *Appl. Phys. Lett.* **65**, 1012 (1994).
- [16] T. Sakamoto *et al.*, *Jpn. J. Appl. Phys.* **33**, 4876 (1994).
- [17] J. A. Katine *et al.*, *Superlattices Microstruct.* **16**, 211 (1994).
- [18] J. M. Martinis and M. Nahum, *Phys. Rev. B* **48**, 18 316 (1993).
- [19] P. D. Dresselhaus *et al.*, *Phys. Rev. Lett.* **72**, 3226 (1994).
- [20] V. Chandrasekhar and R. A. Webb, *Phys. Rev. Lett.* **67**, 2862 (1991).
- [21] A. A. M. Staring *et al.*, *Phys. Rev. B* **45**, 9222 (1992).
- [22] S. W. Huang *et al.*, *Phys. Rev. B* **49**, 16 441 (1994).
- [23] F. R. Waugh, Ph.D thesis, Harvard University, 1994.
- [24] The capacitance per unit length between two thin coplanar rectangular metal strips of width  $w$  and separation  $d$  in a medium with dielectric constant  $\epsilon$  is  $C/L = (2\epsilon/\pi) \ln(2w/d)$  for  $L \gg d$ ; for coplanar circular dots, curved facing edges cut off the log divergence and the interdot capacitance varies slowly with  $d$ .
- [25] K. A. Matveev, L. I. Glazman, and H. U. Baranger (to be published).
- [26] J. M. Golden and B. I. Halperin (to be published).

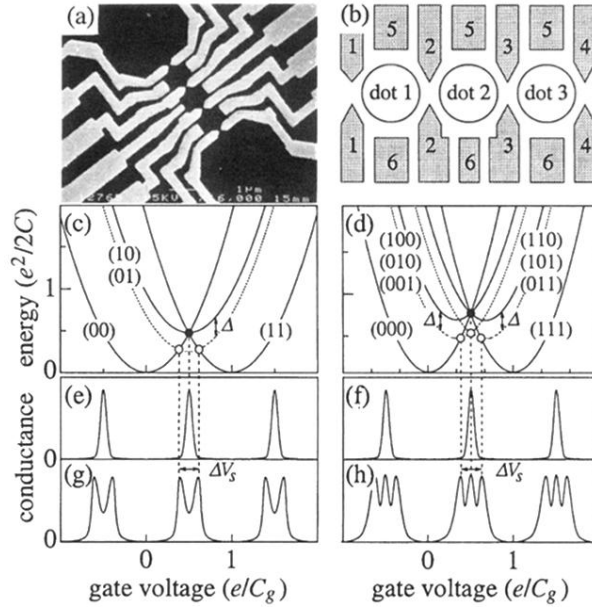


FIG. 1. (a) SEM micrograph at  $16\,000\times$  magnification of three coupled quantum dots with tunable tunneling barriers in GaAs/AlGaAs heterostructure. Scale bar is  $1\,\mu\text{m}$ ; dots are  $0.5 \times 0.8\,\mu\text{m}^2$ . (b) Dot and gate labeling. (c) Double-dot and (d) triple-dot charging energy vs gate voltage for indicated numbers ( $N_1 N_2 \dots$ ) of electrons on each dot for identical dots. Without interdot coupling, parabolas with unequal  $N_i$  are degenerate (solid curves). Coupling removes degeneracy, shifting lowest parabola down by  $\Delta$  (dotted curves). (e) Double-dot and (f) triple-dot conductance vs gate voltage without coupling (schematic). Conductance peaks occur at filled markers in (c) and (d). (g) Double-dot and (h) triple-dot conductance vs gate voltage with coupling (schematic). Conductance peaks occur at open markers in (c) and (d). Coupling splits peaks, with split peak separation  $\Delta V_s \propto \Delta$  for small  $\Delta$ .